Catalyst-free synthesis and deposition mechanism of vertically oriented graphene on aluminum foil using PECVD

Zheqiong Fan,[a] Cong Chen,[a] Fenghong Li,[a] Chaozong Liu,[c] Bo Liu,[*bc] Zhihui Zhang[b]

a College of Materials Science and Engineering, Changsha University of Science and Technology, Changsha, 410114, China

b Key Laboratory of Bionic Engineering, Ministry of Education, Jilin University, Changchun 130022, China

c UCL Institute of Orthopaedics and Musculo-Skeletal Science, M14 the Royal National Orthopaedic Hospital, University College London, Stanmore, HA7 4LP, United Kingdom

E-mail: lbb1107@126.com, lbb1107@jlu.edu.cn (B. Liu).

Abstract

The catalyst-free growth of vertically oriented graphene (VG) networks with growth rate of about 5 nm/min on commercial aluminum (Al) foil via radio frequency plasma-enhanced chemical vapor deposition (RF-PECVD) is reported. The effects of process parameters, including precursor type and deposition temperature, on VG synthesis were systematically investigated. The deposition temperature plays a decisive role in the formation of VGs, while the precursor primarily influences growth rate and crystallinity. VGs were synthesized using either ethylene (C_2H_4) or propylene (C_3H_6) as precursors, but formation does not occur at lower temperatures (e.g., 500 °C). Precursors that effectively generate carbon dimers and exhibit a higher H:C ratio are more favorable

for achieving VGs with high growth rates and superior crystallinity. Furthermore, we proposed a deposition mechanism that encompasses both the growth of VGs on the Al foil surface and the diffusion of carbon atoms into the Al foil. The growth process of VGs follows three distinct stages: the formation of buffer carbon nanoislands, nucleation, and subsequent growth. X-ray photoelectron spectroscopy (XPS) revealed the chemical interactions between carbon, Al_xO_y, and metallic Al at the interface, resulting in a diffusion layer and an interface layer between the VG layer and the underlying Al substrate.

Keywords: vertically oriented graphene, chemical vapor deposition, growth mechanism, precursors

1. Introduction

Cost-effective and lightweight aluminum (Al) foils are widely used as current collectors in various energy storage devices, including electrolytic capacitors, supercapacitors, lithium-ion batteries, and sodium-ion batteries[1, 2]. However, commercial Al foils have intrinsic limitations, such as a limited contact area with active materials, leading to weak adhesion and poor interfacial conductivity. These issues ultimately reduce the rate capability and cycling stability of the devices. To address these deficiencies, several modification strategies have been explored, including surface roughening and the addition of decorative coatings or self-assembled foreign layers[3-6].

Graphene, a two-dimensional honeycomb lattice of sp^2 carbon atoms, is a highly promising coating material for Al current collectors due to its exceptional mechanical,

electrical, optical, and thermal properties[7]. Numerous studies have demonstrated that graphene coatings can significantly enhance the corrosion resistance and conductivity of Al foils[8-10]. For instance, Wang et al. reported that graphene-coated Al foil exhibited markedly improved anodic corrosion resistance, resulting in enhanced electrochemical performance in lithium-ion batteries[11]. However, most studies on graphene-coated Al foils have focused on conventional horizontally oriented graphene (HG) that the sheets are aligned parallel to the substrate. Compared to HG, vertically oriented graphene (VG), whose sheets are perpendicular to the substrate, offers distinctive advantages, including non-agglomerated inter-networked structures, controllable inter-sheet connectivity, high surface-to-mass ratio, and a dense array of atomic-scale graphitic edges[12, 13]. These features make VG an excellent candidate for energy and environmental applications[14, 15]. To our best knowledge, only one report has explored VG-modified Al current collectors, which were successfully applied to high-power sodium-ion batteries[16]. Unfortunately, this study provided no details on the VG preparation process, and the growth mechanism of VG on Al foil without a catalyst remains unclear.

To fully exploit the advantages of VG-coated Al foils, it is critical to achieve the controllable growth of VG with desirable properties, such as high specific surface area, optimized interlayer spacing, and appropriate surface roughness[15, 17]. In this study, VG was directly grown on commercial Al foil without any catalyst using plasma-enhanced chemical vapor deposition (PECVD). The morphology and microstructure of the synthesized VG were thoroughly characterized, and the effects of process

parameters, including deposition temperature and precursor type, were systematically investigated. Additionally, the interfacial structures of VG-Al foils, including the formation of metallurgical bonds, were comprehensively analyzed. The results of this study provide valuable insights into the optimal utilization of VG-coated Al foils for energy storage applications.

2. Experimental sections

2.1 Sample preparation

The PECVD equipment used in our experiment is a home-made horizontal cylinder furnace (Fig. 1), in which three main parts are included: the gas system, the plasma generator and the vacuum heating chamber. The precursor controlled by mass flowmeter was introduced into the furnace from the left. Radio frequency (RF, 13.56 MHz) was used as plasma source. The energy from the RF generator is coupled through the inductive cylindrical coils which surrounded on the quartz tube. In the vacuum heating chamber, three thermocouples were placed evenly to ensure a 400-mm-length region with uniform temperature distribution. The commercial Al foil (3 × 3 cm^2, battery grade, 16 μm, Hefei kejing Material Technology Co., Ltd) substrate was placed at the center of the heating region. Before use, the Al foils were cleaned by acetone solution and ethanol solution successively, and then the foils were dried by nitrogen. The procedure was repeated by three times. The detailed PECVD process parameters were listed as follows: the deposition was conducted at 500~600 °C with pressure of 50 Pa. Ethylene (C_2H_4, 99.9%) and propylene (C_3H_6, 99.9%) without a diluent were used as precursors, respectively. The flow rate of the precursor was 50 sccm, and the plasma

power was 350 W. The deposition lasted for 20~60 min. The furnace was under a nitrogen atmosphere during both the heating and cooling processes. Additionally, a piece of Al foil was used for a second growth under the same condition after sonication in acetone for 6 h.

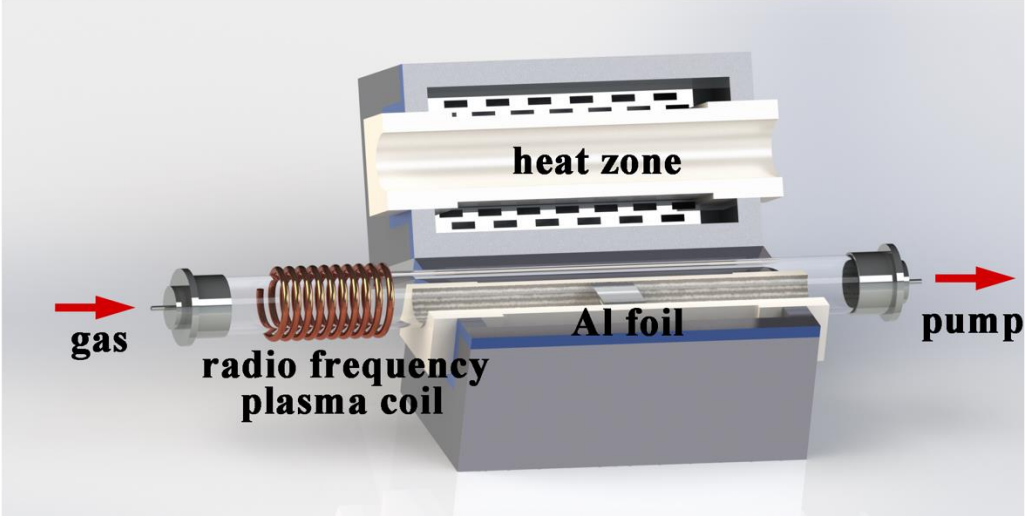

Fig. 1 Schematic diagram of the apparatus for the preparation of VGs

2.2 Characterizations

Scanning electron microscope (SEM, JEOL JSM-IT700HR) equipped with energy dispersive spectroscopy (EDS) was used to examine both the morphologies and compositions of the products. The structural informations were acquired by Raman spectroscopy (Renishaw inVia Qontor) and high resolution transmission electron microscope (HRTEM, FEI Tecnai F20). The curve fitting of the first-order Raman spectra (1000~2000 cm^{-1}) for the determination of spectral parameters was performed with the software program Origin 2020 by using the procedure proposed by Sadezky et al[18]. The TEM specimens were prepared by ultrasonic method. That is, the VGs-Al foil developed was immersed in ethanol solution to ultrasonic for 4 h. Then, a few drops

of ethanol solution in which contains VGs were added on a 3 mm-diameter copper mesh. After evaporation of ethanol, the TEM specimen of VGs was finished. The interfacial composition and distribution of sonicated VGs-Al foil and primary Al foil were determined by X-ray photoelectron spectroscopy (XPS, PHI VersaProbe 4) analysis with Ar-ion sputter etching. The three-dimensional topography of samples were characterized by a 3D scanner (GOM ATOS Scanbox 4105).

3. Results and discussion

The choice of precursor plays a critical role in determining the morphology and properties of VG grown via the PECVD process[7, 19]. While a wide range of precursors, including hydrocarbons, fluorocarbons, carbon oxides, and natural solid or liquid materials, have been explored, volatile small hydrocarbons (CH_4, C_2H_2 and C_2H_4) remain the most used[12, 20-23]. However, C_3H_6, a gaseous alkene that serves as the primary carbon source for pyrolytic carbon deposition, has rarely been applied to VG synthesis. In this study, C_2H_4 and C_3H_6 were selected as precursors for VG growth. After 60 minutes of deposition, both precursors produced uniform and continuous carbon coatings on Al foils (Fig. S1), resulting in a change in the macroscopic appearance of the Al foil from silvery white to dark gray. The microscopic morphologies of the as-prepared carbon-coated Al foils remained largely unchanged compared to the original Al foil, with rolling lines and holes still clearly visible (Fig. S1).

As shown in the SEM images in Fig. 2, typical VG structures were observed in the carbon coatings produced by both precursors. Interconnected carbon sheets, several

nanometers thick, were oriented vertically to the Al foil, and their distribution was remarkably uniform across the substrate surface. The top edges of the carbon sheets appeared brighter than the base areas, indicating that the top layers were thinner than those at the base. Despite both coatings consisting of VGs, differences were observed between the samples: the VGs synthesized using C_3H_6 were finer and more delicate than those grown using C_2H_4.

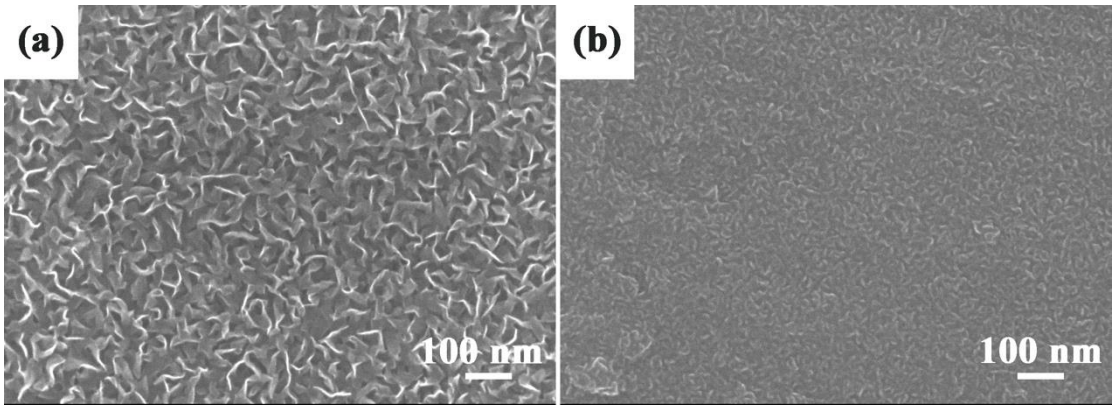

Fig. 2 Surface SEM images of the deposits prepared by (b) C_2H_4 and (c) C_3H_6 at 600 °C with deposition time of 60 min

The typical Raman spectra of the as-prepared VGs are shown in Fig. 3. Three prominent bands are observed: the D band (~1350 cm^{-1}), G band (~1580 cm^{-1}) and G' band (~2700 cm^{-1}). The D band is induced by defects in the crystal structure, while the G band arises from vibrations between neighboring carbon atoms within the graphene plane[18]. The G' band, on the other hand, originates from the double-resonance Raman process, which occurs without any defects[24]. Additionally, a weak disorder-induced D' band appears at ~1620 cm^{-1} as a shoulder of the G band. The intensity ratio of the D band to the G band (I_D/I_G) is commonly used to evaluate the level of crystallinity, as it

is inversely proportional to the degree of crystallinity[18]. From Fig. 3, the I_D/I_G values for the VGs samples prepared using C_2H_4 and C_3H_6 are 1.72 and 1.39, respectively. These high I_D/I_G values indicate that the crystallinity of the obtained VGs is low, with the VGs prepared from C_2H_4 exhibiting a lower degree of crystallinity. This is primarily attributed to the significant number of defects arising from the abundant exposed edges of the graphene sheets, as confirmed by the sharp profile and high intensity of the D band. These exposed edges are critical for VGs' applications in field emitters, gas sensors, and biosensors[13, 17]. The structural analysis derived from the first-order Raman spectra aligns well with the results obtained from SEM observations.

Another notable feature of the graphene Raman spectra is the G' band, whose spectral shape provides insights into the number of layers and stacking order within the nanosized graphene sheets[25, 26]. Previous studies have demonstrated that the G' band evolves with an increase in graphene layers: it changes from a single sharp line (monolayer graphene) to multiple lines (multilayer graphene) and eventually to a broader single line (turbostratic graphite)[24, 25]. The insets in Fig. 3 highlight the details of the G' region, where a symmetric G' signal is observed, requiring only a single Lorentzian profile to fit the experimental data. The full width at half maximum (FWHM) values of the G' bands range from 90 to 110 cm^{-1}, significantly wider than the FWHM of monolayer graphene (~24 cm^{-1})[26]. These observations suggest that the as-prepared VGs consist of multilayer graphene with a turbostratic random stacking configuration.

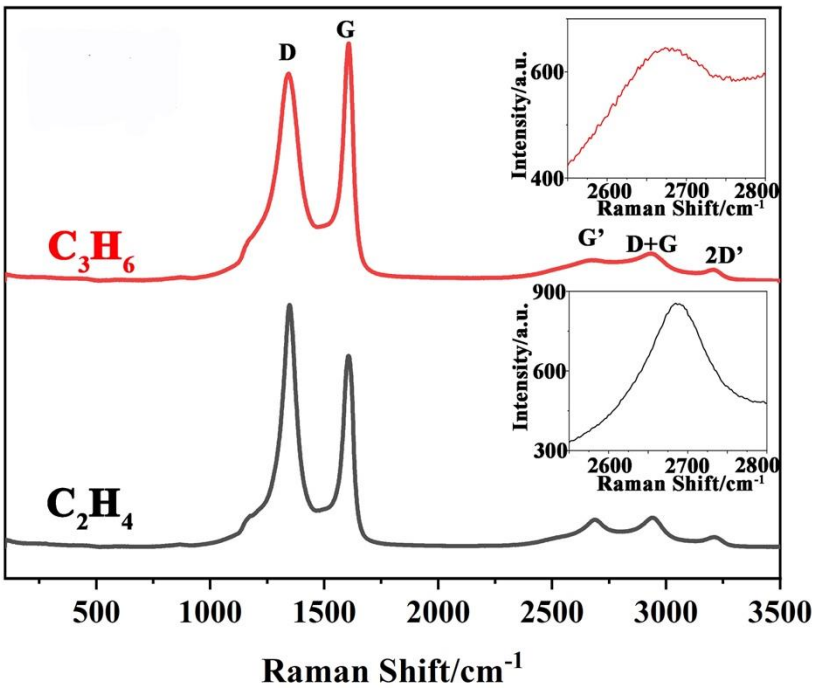

Fig. 3 Raman spectra of VGs prepared by C_2H_4 and C_3H_6, respectively. The insets are the magnification of G' band.

Given that VGs were successfully synthesized using both C_2H_4 and C_3H_6 as carbon sources, it can be concluded that the choice of gas precursor is not the primary parameter governing VG growth. The feedstock gas significantly influences the synthesis process, affecting the morphology, structure, and growth rate of the resulting deposits[27-29]. It is widely accepted that reactive carbon dimers in the deposition zone play a crucial role in the evolution of critical nuclei into VG sheets[12, 30, 31]. Therefore, CH_4 and C_2H_2, which are effective providers of carbon dimers, are the most used precursors for VG synthesis. Among these, C_2H_2 is preferred due to the strength of the C≡C bond, which facilitates easier production of carbon dimers compared to CH_4[17]. Consequently, VGs grow more rapidly when using C_2H_2 as the feedstock. Moreover, some researchers have suggested that C_3-type radicals serve as the

fundamental building blocks for VGs growth[32]. In our case, the primary pyrolysis products of C_2H_4 and C_3H_6 were found to be C2 and C3 species, respectively[33]. This indicates a higher density of carbon dimers in the C_2H_4 plasma, which promotes the formation of VGs with larger graphene sheets. Furthermore, while no additional diluent gases (H_2, N_2, Ar) were introduced into the PECVD system, the hydrogen atoms present in the hydrocarbon precursors (C_2H_4 and C_3H_6) likely acted as etching agents[23, 34]. Hydrogen atoms or radicals generated in the plasma can reduce defects in VGs during growth. As a result, the higher hydrogen content in C_3H_6 promotes the formation of VGs with a lower I_D/I_G value. However, the etching effect is limited by the relatively low hydrogen content in the system.

The detailed microstructural features of the as-prepared VGs were investigated using HRTEM, with the corresponding results shown in Fig. 4. A small piece of bulk VG film, measuring several micrometers, can be seen in Fig. 4a, indicating that the binding force between the graphene sheets is strong enough to withstand ultrasonic wave disruption. The periphery of the film consists of numerous curved graphene sheets with a petal-like appearance. A closer examination of these graphitic petals reveals two distinct types of edges at the tips: faceted edges and open edges, as highlighted by arrows of different colors in Fig. 4b. The faceted edges are formed by folding graphene, typically at zigzag or armchair positions, as evidenced by angle measurements between folds quantized at approximately 30º[35, 36]. In contrast, open edges, also referred to as non-faceted edges, represent areas where growth can occur. Fig. 4c shows a typical TEM image of a graphitic sheet with multiple folds. The edge contrast of the faceted

edges is apparent due to the thickness variation from the folded flaps. It is generally accepted that the structural stability of a vertical graphitic sheet decreases as its size increases[35]. Thus, it is speculated that as a vertical graphitic sheet grows larger, its edges may collapse due to reduced structural stability, forming folds, and changing orientation by approximately 30º. Repeated folding can occur within a single graphene petal, resulting in multiple facets in 2D projections and a curvy surface in 3D topography. These folded edges provide mechanical stability to the graphitic petals, helping to maintain the vertical structure during growth. Additionally, the growth rate varies along different positions of the open edges, creating a wavy profile. The HRTEM image (Fig. 4d) reveals that the petals consist of several stacked graphitic layers with an interlayer spacing of approximately 0.34 nm. Amorphous carbon is also observed between the petals, which contributes to the D band observed in the Raman spectra.

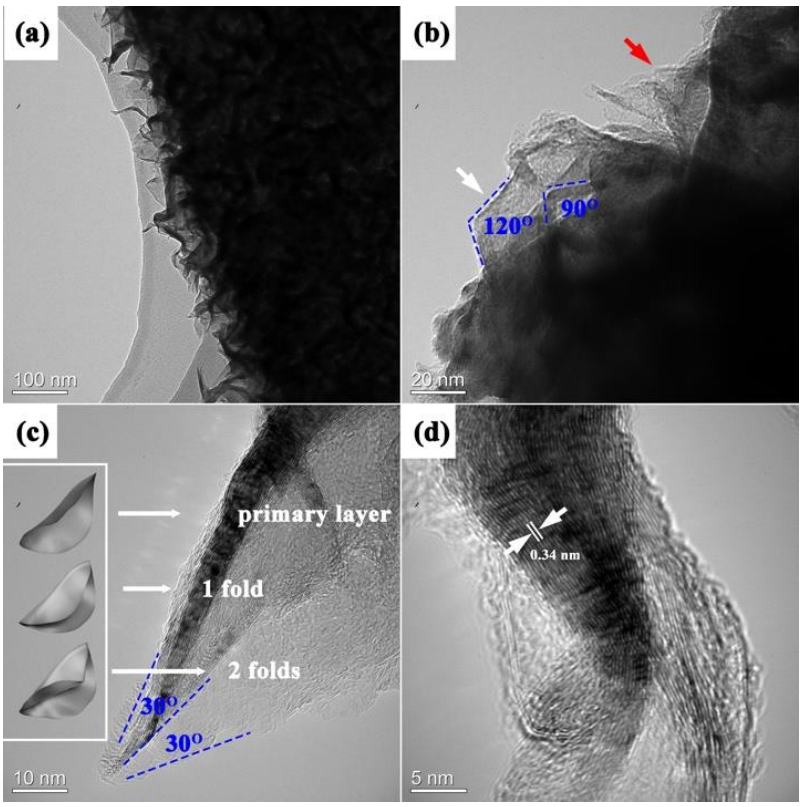

Fig. 4 TEM images of VGs prepared by C_2H_4 at 600 °C with deposition time of 60 min. The white arrow points to a facetted edge, while the red arrow points to an open edge in (b). The inset in (c) is the simulation of 3D topography.

Deposition temperature is one of the most critical process parameters influencing the growth of VGs, since it strongly affects the kinetics of pyrolysis reactions and surface reactions. Fig. 5 presents the SEM surface analysis of the Al foil substrate after deposition at various temperatures. At a deposition temperature of 500 °C, no VG film was formed, as shown in Fig. 5a. Instead, the Al foil substrate was uniformly covered with nanoislands ranging in size from 20 nm to 60 nm. Additionally, some vertical flakes, approximately 10–30 nm in length, were observed at the edges of the nanoislands (marked by arrows in Fig. 5a). These sparse vertical flakes indicated that the growth was still in the nucleation stage at this temperature, while the underlying nanoislands served as the buffer layer. When the deposition temperature increased to 600 °C, the growth of a VG film became evident after 20 minutes of deposition (Fig. 5b). A substantial number of vertical carbon flakes, several nanometers thick (Fig. S2) and tens of nanometers long, formed across the Al foil substrate. The dense flakes, which appeared both straight and curved, suggest that the growth had progressed to the rapid growth stage with a growth rate of about 5 nm/min. From the temperature comparison experiments, under the influence of PE, the precursor gas can decompose at lower temperatures to generate C2 radicals. However, when the deposition temperature is too low, the concentration of active species in the deposition atmosphere

is insufficient to support the formation of VGs.

The Raman spectra of the VGs synthesized at different temperatures are presented in Fig. 5c. Based on the decreasing I_D/I_G values, from 2.0 at 500 °C to 1.92 at 600 °C, it can be inferred that the degree of crystallinity in the deposits increased with the rise in deposition temperature. Although both Raman spectra exhibit a D band with high intensity, the primary causes of the D band differ significantly. For the deposit prepared at 600 °C, the D band was predominantly caused by the abundance of open edges in the VGs. In contrast, the deposit prepared at 500 °C showed defects primarily attributed to internal crystalline imperfections, such as vacancies and disorders, which are likely due to the lower deposition temperature. At lower temperatures, the depositing species may have limited mobility, preventing them from rearranging into a preferred structure[37]. Compared to the Raman spectra in Fig. 3, it appears that the crystallinity of the VGs improved with increased deposition time. Additionally, the appearance of a characteristic G' peak in the sample prepared at 500 °C suggests that the nanoislands consisted of finite-sized sp^2-hybridized crystallites oriented parallel to the substrate surface.

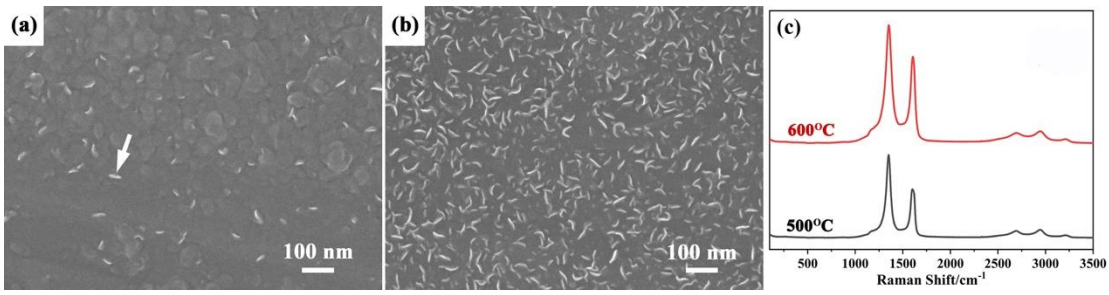

Fig. 5 Surface SEM images of deposits prepared at (a) 500 °C and (b) 600 °C. Raman spectra of deposits prepared at 500 °C and 600 °C by using C_2H_4 as precursor with the

deposition time of 20 min.

To further investigate the interface between the Al substrate and the VGs film, additional experiments were conducted. After the initial growth, the Al substrate was reused by carefully removing the synthesized VGs in an ultrasonic bath. The surface SEM images and corresponding EDS results of the VGs-Al sample after sonication treatment are shown in Fig. 6. A few isolated VG residues with irregular shapes and varying sizes were still observed on the Al substrate, indicating the formation of a stable cohesion between the VGs and the Al substrate. As shown in Fig. 6b, in addition to the Al and O elements, a small amount of uniformly distributed C was detected in the uncovered regions of the Al foil. However, the concentration of C in these regions was significantly lower compared to the covered areas. This suggests that an interface layer was formed between the Al substrate and the VGs, likely due to diffusion or chemical reactions.

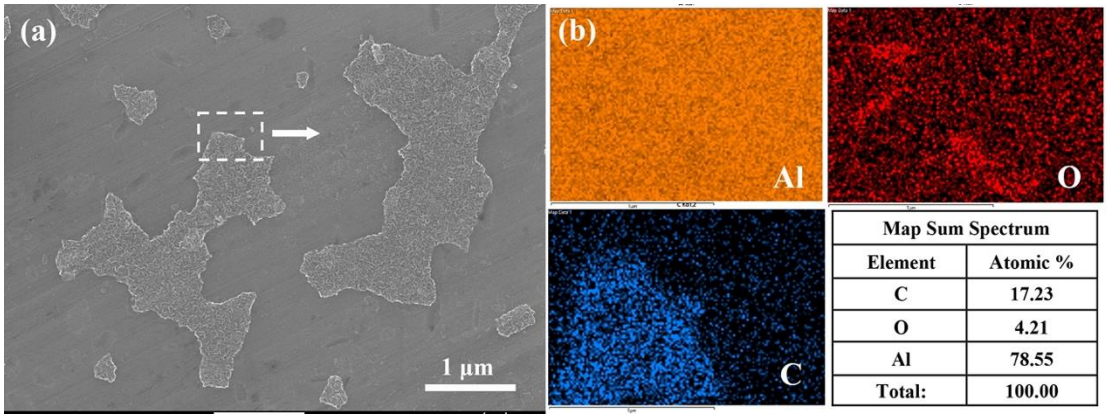

Map Sum Spectrum	
Element	Atomic %
C	17.23
O	4.21
Al	78.55
Total:	100.00

Fig. 6 (a) surface SEM image and (b) corresponding EDS results of the VGs-Al sample after sonication treatment.

SEM images of VGs grown on a reused Al foil were collected and are shown in

Fig. 7. After the first VGs synthesis and subsequent removal, VGs were successfully regrown on the reused Al substrate during a second growth process. No significant differences were observed in the morphology or density of the VGs films between the first and second growth cycles. The interface layer formed on the Al foil surface during the deposition process has little effect on the re-growth of the second round of VGs. In other words, the growth of VGs is not limited by the surface state of the Al foil. This indicates that additional surface treatments such as acid pickling or preoxidation, which are typically required for metal substrates to deposit nanocarbon materials, are not needed for reusing Al substrates in VG synthesis. However, a distinct boundary between the newly grown VG region and the primary VG region was observed, caused by a height difference in the deposition substrate. During the second growth process, some active intermediate products adsorbed onto the reused Al substrate surface to form new VGs, while others adsorbed onto the edges of the topmost graphene sheets in the residual VGs, extending the existing graphene layers. Consequently, the graphene sheets in the primary VG region were larger than those in the newly grown VG region, as shown in Fig. 7b. The height difference between the newly grown and primary VGs was measured to be in the range of 0.6 μm to 1.1 μm (Fig. S3).

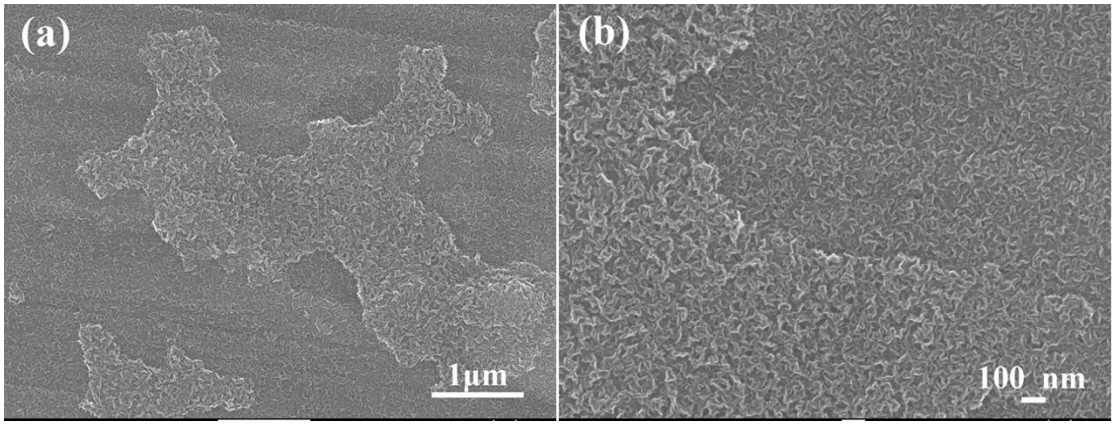

Fig. 7 Surface SEM images of VGS grown on a reused Al foil

XPS was performed to further probe the interface between VGs and Al substrate. The XPS wide scan spectra of primary Al foil (P-Al) and sonicated VGs-Al substrate (S-VGs-Al) indicated that there are only Al, O and C are present. The atom percentages of these three elements in depth revealed by Ar-ion sputter etching are shown in Fig. 8. From Fig. 8a, mainly C, O and a small amount of Al are present at the fresh P-Al surface. After 30 s of sputtering, the amount of C dramatically decreased from 42.5% to 2.6% and maintained at a relative stable low level (3.5%) as etching progressing. By contrast, the percentage of Al increased significantly from 16.3% to 73.0% in the etch process. And the gradually decreasing atomic percentage ratio of O to Al suggesting a gradient compositional variation in the Al oxide film. So Al_xO_y rather than Al_2O_3 was more suitable to represent the component of oxide thin film on Al foil. Fig. 8b shows the depth profiling of Al, O and C (at.) in S-VGs-Al. The percentage of C maintained at a predominant level (high than 60%) throughout due to the residual VGs on surface. According to the distribution of Al and O in depth, three layers can be divided, that is surface VGs layer, diffusion layer and interface layer. The three layers are schematically illustrated in Fig. 8b. Surface VGs layer mainly consist of C. In the diffusion layer, percentages of Al and O gradually increase, and the proportion of O is slightly higher than that of Al. For the interface layer, percentage of Al keeps increase from 12.6% to 16.8%, while that of O begins to decrease from 22.9% to 5.3%.

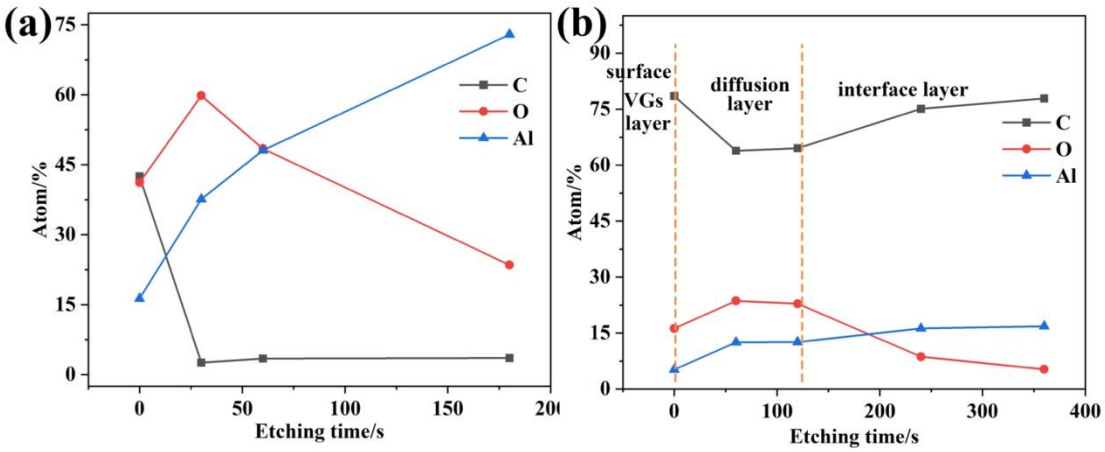

Fig. 8 Depth profiling of C, O and Al (at.) in (a) P-Al and (b) S-VGs-Al during Ar-ion sputter etching

Fig. 9 presents high-resolution XPS scans of Al 2p and C 1s for S-VGs-Al after different durations of Ar-ion sputter etching. The Al 2p and C 1s peaks were fitted to species with different valences, and the percentages of these species (calculated based on the area ratios of the fitted peaks) are provided in Table S1. In Fig. 9a, the Al 2p scans are deconvoluted into peaks centered at approximately 75 eV (Al_xO_y), 74 eV (Al-O-C), 73 eV (Al-C), and 72.7 eV (Al metal)[38, 39]. These four peaks are present throughout the depth profile. Among them, Al_xO_y and Al metal represent the original components of the Al oxide film and Al substrate, respectively. In contrast, Al-O-C and Al-C are identified as reaction products formed by the interaction of carbon diffused from the surface VG layer with Al_xO_y or Al metal, as described in reaction path (1), (2), and (3) below[39].

$$Al_xO_y + C \rightarrow Al - O - C \quad (1)$$

$$Al - O - C + C \rightarrow Al - C \quad (2)$$

$$Al + C \rightarrow Al - C \quad (3)$$

Al_xO_y and Al-O-C dominate the diffusion layer, where Al_xO_y increases from 47.6% to 79.6%, while Al-O-C and Al-C decrease (Al-O-C: 41.0% to 12.5%; Al-C: 7.3% to 1.0%). This reflects a carbon concentration gradient, with the highest Al-C and Al-O-C near the surface. Al metal remains steady (6.4%–8.9%), suggesting Al-C in this layer forms via reaction path (2).

In the interface layer, Al-C and Al metal increase significantly (Al-C: 1.0% to 15.6%; Al metal: 6.9% to 39.0%), indicating Al-C forms primarily via reaction path (3). Fig. 9b shows C 1s peaks at ~285.2 eV (C-O), ~284.4 eV (C-C), and ~283 eV (Al-O-C), with C-C and C-O as the major species[38, 39]. At an etch time of 360 seconds, trace Al-C species appear in the interface layer.

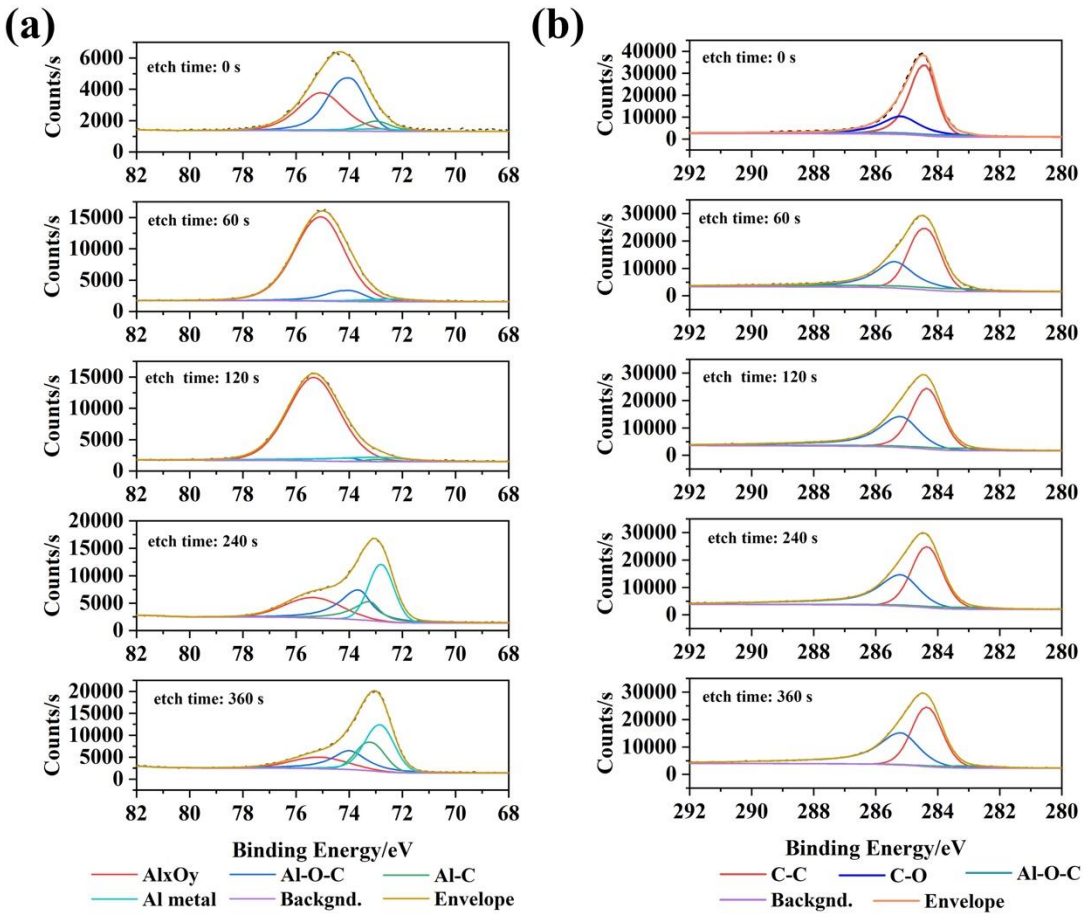

Fig. 9 XPS spectra and peak fittings of S-VGs-Al sample in depth profile, (a) Al 2p

345 scan, (b) C 1s scan

346

347 Based on the results, the deposition model schematically illustrated in Fig. 10 is
348 proposed. When the precursor (C_2H_4 or C_3H_6) is introduced into the plasma, the
349 generated C_xH_y ions and radicals adsorb onto the surface of the Al foil. Through a series
350 of gas-solid heterogeneous reactions, carbon atoms are captured while gaseous H_2 is
351 desorbed. Some of these captured carbon atoms deposit on the Al foil surface to form
352 VGs, while others diffuse into the Al foil substrate. Initially, a buffer layer of carbon
353 nanoislands with numerous crystalline defects forms on the Al foil surface[40].
354 Subsequently, carbon flakes at the edges of the nanoislands begin to grow upward to
355 release internal stress caused by lattice mismatch between the Al substrate and the
356 buffer layer[19], serving as nucleation sites and transitioning the growth direction from
357 planar to vertical. In the final stage, dissociated carbon species continuously adsorb
358 onto the surface of vertically growing carbon sheets, moving rapidly until covalently
359 bonding with edge carbon atoms. Carbon dimers act as the primary building blocks for
360 VGs, and as the vertical carbon sheets expand, their structural stability weakens,
361 causing edge collapse and forming the characteristic petal-like morphology.

362 For the diffusion process, carbon atoms diffuse into the Al substrate and react with
363 Al_xO_y and Al metal to form Al-O-C and Al-C species, respectively. The concentration
364 of Al-O-C decreases with depth, while Al-C increases, suggesting the existence of a
365 diffusion layer and an interface layer between the VG top layer and the pure Al substrate.
366 This dual process of deposition and diffusion not only provides strong adhesion

between the VGs and the Al foil substrate but also helps reduce the interfacial resistance of the Al foil[41].

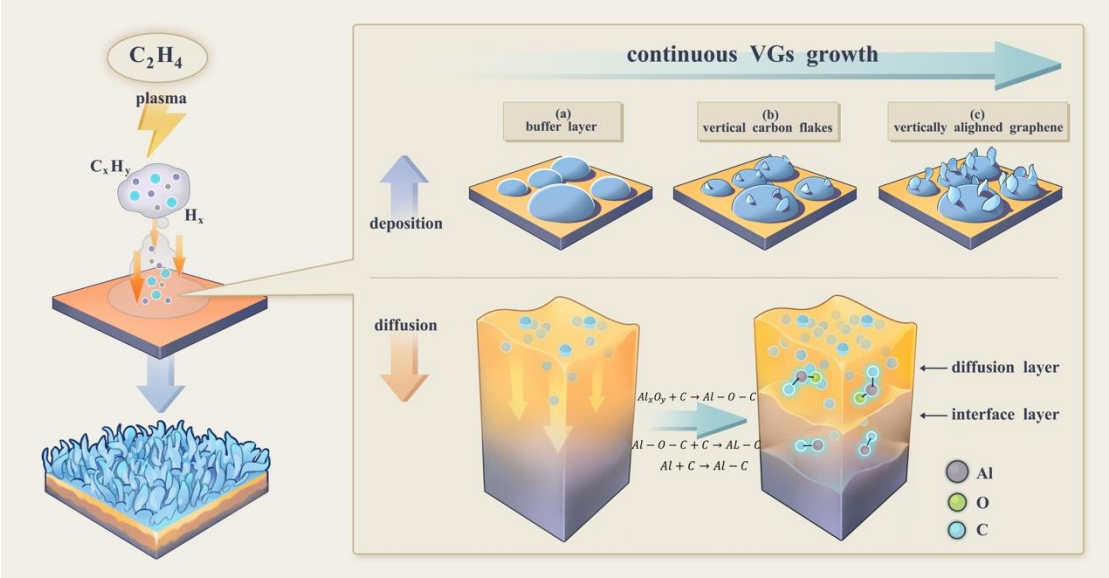

Fig. 10 Deposition process of VGs on Al foil

Taken together, we present a novel PECVD process for the growth of VGs on Al foil, offering insights into the deposition mechanism and its application potential. The proposed three-stage growth process—buffer layer formation, nucleation of vertical carbon flakes, and VG growth—was found to be consistent across different precursors (C_2H_4 and C_3H_6) and temperatures. However, the duration of each stage is highly dependent on process parameters. Low temperatures or reduced concentrations of active species extend the buffer layer deposition or nucleation stages, indicating the need for optimized conditions to achieve efficient VG growth.

The formation of nanoislands as the buffer layer on Al foil is a notable finding, differing from previously reported carbides, amorphous carbon, or graphene layers observed on other substrates. Further investigation into the internal structure of these

nanoislands is essential for understanding their role in VG growth and improving the synthesis process.

The dual deposition and diffusion mechanism ensures strong adhesion and low interfacial resistance, making the VGs-Al composite highly suitable for applications in energy storage devices such as supercapacitors, lithium-ion batteries, and sodium-ion batteries. The robust process, which avoids thermal damage and eliminates the need for additional substrate treatments, enhances the scalability and economic viability for industrial applications. These findings not only deepen the understanding of VG growth mechanisms but also expand the potential application areas of Al foils in advanced energy and electronic devices.

4 Conclusion

In summary, petal-like VGs were successfully synthesized on commercial Al foil via catalyst-free PECVD. The as-prepared VG networks consisted of vertical oriented curvy carbon petals with a thickness of several nanometers. In each carbon petal, a few of graphene sheets were stacked in parallel with interlayer spacing of 0.34 nm. Multiple folds were formed in these petals during growth, in order to maintain the stability of the vertical structure. While the choice of precursor and the presence of gaseous etchants did not critically affect VG formation, they influenced growth rate, size, and crystallinity. Nevertheless, deposition temperature is of importance in VG's growth. VG film cannot be deposited at a low temperature (500 °C). Finally, the growth mechanism of VGs on Al foil was revealed, involving three stages: the formation of a buffer carbon layer, the nucleation stage, and the final growth of dense VG networks.

Acknowledgements

The authors would like to gratefully acknowledge the Changsha Natural Science Foundation of China for Award No. kq2402033, Opening Project of Engineering Research Center of Eco-friendly Polymeric Materials, Ministry of Education and Open Research Fund of state Key Laboratory of Polymer Physics and Chemistry, Changchun Institute of Applied Chemistry Chinese Academy of Sciences for supporting this research.

References

[1] C. Behling, J. Lüchtefeld, S.J. Wachs, K.J.J. Mayrhofer, B.B. Berkes, Quantifying the influence of temperature on Al current collector dissolution in LiTFSI-based lithium-ion battery electrolytes via coupled on-line mass analysis, Electrochimica Acta 473 (2024) 143480. https://doi.org/10.1016/j.electacta.2023.143480.

[2] Y. Peng, X. Feng, J. Xia, Z. You, F. Zhang, Y. Chen, C. Fan, J. Hua, Y. Lian, Z. Shan, M. Ouyang, Polymer based multi-layer Al composite current collector improves battery safety, Chemical Engineering Journal 491 (2024) 151474. https://doi.org/10.1016/j.cej.2024.151474.

[3] D.Y. Shin, D.H. Park, H.J. Ahn, Interface modification of an Al current collector for ultrafast lithium-ion batteries, Applied Surface Science 475 (2019) 519-523. https://doi.org/10.1016/j.apsusc.2019.01.016.

[4] P. Tallone, S. Spriano, D. Versaci, S. Ferraris, A. Tori, S. Bodoardo, Picosecond laser texturing of Al current collector to improve cycling performances and simplify recycling of Lithium-ion batteries, Surfaces and Interfaces 51 (2024) 104659.

https://doi.org/10.1016/j.surfin.2024.104659.

[5] G. Teucher, T. Van Gestel, M. Krott, H.G. Gehrke, R.A. Eichel, S. Uhlenbruck, Processing of Al-doped ZnO protective thin films on aluminum current collectors for lithium ion batteries, Thin Solid Films 619 (2016) 302-307. https://doi.org/10.1016/j.tsf.2016.10.047.

[6] H.C. Wu, Y.P. Lin, E. Lee, W.T. Lin, J.K. Hu, H.C. Chen, N.L. Wu, High-performance carbon-based supercapacitors using Al current-collector with conformal carbon coating, Materials Chemistry and Physics 117(1) (2009) 294-300. https://doi.org/10.1016/j.matchemphys.2009.06.001.

[7] V.P. Pham, H.S. Jang, D. Whang, J.Y. Choi, Direct growth of graphene on rigid and flexible substrates: progress, applications, and challenges, Chemical Society Reviews 46(20) (2017) 6276-6300. https://doi.org/10.1039/c7cs00224f.

[8] J. Liu, L. Hua, S. Li, M. Yu, Graphene dip coatings: An effective anticorrosion barrier on aluminum, Applied Surface Science 327 (2015) 241-245. https://doi.org/10.1016/j.apsusc.2014.11.187.

[9] D. Wei, M.R. Astley, N. Harris, R. White, T. Ryhänen, J. Kivioja, Graphene nanoarchitecture in batteries, Nanoscale 6(16) (2014) 9536-9540. https://doi.org/10.1039/c4nr02089h.

[10] Y. Zhao, B. Liu, Y. Yi, X. Lian, M. Wang, S. Li, X. Yang, J. Sun, An Anode-Free Potassium-Metal Battery Enabled by a Directly Grown Graphene-Modulated Aluminum Current Collector, Advanced Materials 34(29) (2022) 2202902. https://doi.org/10.1002/adma.202202902.

449 [11] M. Wang, M. Tang, S. Chen, H. Ci, K. Wang, L. Shi, L. Lin, H. Ren, J. Shan, P.
450 Gao, Z. Liu, H. Peng, Graphene-Armored Aluminum Foil with Enhanced Anticorrosion
451 Performance as Current Collectors for Lithium-Ion Battery, Advanced Materials 29(47)
452 (2017) 1703882. https://doi.org/10.1002/adma.201703882.
453 [12] Z. Bo, Y. Yang, J. Chen, K. Yu, J. Yan, K. Cen, Plasma-enhanced chemical vapor
454 deposition synthesis of vertically oriented graphene nanosheets, Nanoscale 5(12) (2013)
455 5180-5204. https://doi.org/10.1039/c3nr33449j.
456 [13] W. Zheng, X. Zhao, W. Fu, Review of Vertical Graphene and its Applications, ACS
457 Applied Materials & Interfaces 13(8) (2021) 9561-9579.
458 https://doi.org/10.1021/acsami.0c19188.
459 [14] P.V. Shinde, R. Samal, C.S. Rout, Vertically Aligned Graphene-Analogous Low-
460 Dimensional Materials: A Review on Emerging Trends, Recent Developments, and
461 Future Perspectives, Advanced Materials Interfaces 9(9) (2022) 2101959.
462 https://doi.org/10.1002/admi.202101959.
463 [15] F. Zhou, J. Shan, L. Cui, Y. Qi, J. Hu, Y. Zhang, Z. Liu, Direct Plasma-Enhanced-
464 Chemical-Vapor-Deposition Syntheses of Vertically Oriented Graphene Films on
465 Functional Insulating Substrates for Wide-Range Applications, Advanced Functional
466 Materials 32(42) (2022) 2202026. https://doi.org/10.1002/adfm.202202026.
467 [16] K. Wang, C. Wang, H. Yang, X. Wang, F. Cao, Q. Wu, H. Peng, Vertical graphene
468 nanosheetsmodified Al current collectors for high-performance sodium-ion batteries,
469 Nano Research 13(7) (2020) 1948-1954. https://doi.org/10.1007/s12274-020-2780-2.
470 [17] Z. Bo, S. Mao, Z. Jun Han, K. Cen, J. Chen, K. Ostrikov, Emerging energy and

environmental applications of vertically-oriented graphenes, Chemical Society Reviews 44(8) (2015) 2108-2121. https://doi.org/10.1039/c4cs00352g.

[18] A. Sadezky, H. Muckenhuber, H. Grothe, R. Niessner, U. Pöschl, Raman microspectroscopy of soot and related carbonaceous materials: Spectral analysis and structural information, Carbon 43(8) (2005) 1731-1742. https://doi.org/10.1016/j.carbon.2005.02.018.

[19] Z. Wu, E. Wang, G. Zhang, Y. Shen, G. Shao, Recent Progress of Vertical Graphene: Preparation, Structure Engineering, and Emerging Energy Applications, Small 20(15) (2023) 2307923. https://doi.org/10.1002/smll.202307923.

[20] S. Sahoo, G. Sahoo, S.M. Jeong, C.S. Rout, A review on supercapacitors based on plasma enhanced chemical vapor deposited vertical graphene arrays, Journal of Energy Storage 53 (2022) 105212. https://doi.org/10.1016/j.est.2022.105212.

[21] M.V. Jacob, R.S. Rawat, B. Ouyang, K. Bazaka, D.S. Kumar, D. Taguchi, M. Iwamoto, R. Neupane, O.K. Varghese, Catalyst-Free Plasma Enhanced Growth of Graphene from Sustainable Sources, Nano Letters 15(9) (2015) 5702-5708. https://doi.org/10.1021/acs.nanolett.5b01363.

[22] A. Al-Jumaili, M.A. Zafar, K. Bazaka, J. Weerasinghe, M.V. Jacob, Bactericidal vertically aligned graphene networks derived from renewable precursor, Carbon Trends 7 (2022) 100157. https://doi.org/10.1016/j.cartre.2022.100157.

[23] Z. Zhang, C.S. Lee, W. Zhang, Vertically Aligned Graphene Nanosheet Arrays: Synthesis, Properties and Applications in Electrochemical Energy Conversion and Storage, Advanced Energy Materials 7(23) (2017) 1700678.

https://doi.org/10.1002/aenm.201700678.

[24] L.M. Malard, M.A. Pimenta, G. Dresselhaus, M.S. Dresselhaus, Raman spectroscopy in graphene, Physics Reports 473(5-6) (2009) 51-87. https://doi.org/10.1016/j.physrep.2009.02.003.

[25] S.S. Nanda, M.J. Kim, K.S. Yeom, S.S.A. An, H. Ju, D.K. Yi, Raman spectrum of graphene with its versatile future perspectives, TrAC Trends in Analytical Chemistry 80 (2016) 125-131. https://doi.org/10.1016/j.trac.2016.02.024.

[26] W. Yao, H. Liu, J. Sun, B. Wu, Y. Liu, Engineering of Chemical Vapor Deposition Graphene Layers: Growth, Characterization, and Properties, Advanced Functional Materials 32(42) (2022) 2202584. https://doi.org/10.1002/adfm.202202584.

[27] Z. Chen, Y. Qi, X. Chen, Y. Zhang, Z. Liu, Direct CVD Growth of Graphene on Traditional Glass: Methods and Mechanisms, Advanced Materials 31(9) (2018) 1803639. https://doi.org/10.1002/adma.201803639.

[28] D.G. Sangiovanni, G.K. Gueorguiev, A. Kakanakova-Georgieva, Ab initio molecular dynamics of atomic-scale surface reactions: insights into metal organic chemical vapor deposition of AlN on graphene, Physical Chemistry Chemical Physics 20(26) (2018) 17751-17761. https://doi.org/10.1039/C8CP02786B

[29] D.G. Sangiovanni, R. Faccio, G.K. Gueorguiev, A. Kakanakova-Georgieva, Discovering atomistic pathways for supply of metal atoms from methyl-based precursors to graphene surface, Physical Chemistry Chemical Physics 25(1) (2022) 829-837. https://doi.org/10.1039/D1CP04009J

[30] A.N. Obraztsov, A.A. Zolotukhin, A.O. Ustinov, A.P. Volkov, Y. Svirko, K. Jefimovs, DC discharge plasma studies for nanostructured carbon CVD, Diamond and Related Materials 12(3-7) (2003) 917-920. https://doi.org/10.1016/s0925-9635(02)00338-2.

[31] N. Soin, S.S. Roy, T.H. Lim, J.A.D. McLaughlin, Microstructural and electrochemical properties of vertically aligned few layered graphene (FLG) nanoflakes and their application in methanol oxidation, Materials Chemistry and Physics 129(3) (2011) 1051-1057. https://doi.org/10.1016/j.matchemphys.2011.05.063.

[32] S. Vizireanu, S.D. Stoica, C. Luculescu, L.C. Nistor, B. Mitu, G. Dinescu. Plasma techniques for nanostructured carbon materials synthesis. A case study: carbon nanowall growth by low pressure expanding RF plasma. Plasma Sources Science and Technology 19(3) (2010) 034016. https://doi.org/10.1088/0963-0252/19/3/034016.

[33] K. Norinaga, O. Deutschmann, K.J. Hüttinger, Analysis of gas phase compounds in chemical vapor deposition of carbon from light hydrocarbons, Carbon 44(9) (2006) 1790-1800. https://doi.org/10.1016/j.carbon.2005.12.050.

[34] X. Gao, R. Xiao, Y. Zhang, Z. Chen, H. Kang, S. Wang, S. Zhao, Y. Sui, G. Yu, W. Zhang, Etching effect of hydrogen and oxygen on the chemical vapor deposition graphene on Cu, Thin Solid Films 758 (2022) 139436. https://doi.org/10.1016/j.tsf.2022.139436.

[35] K. Davami, M. Shaygan, N. Kheirabi, J. Zhao, D.A. Kovalenko, M.H. Rümmeli, J. Opitz, G. Cuniberti, J.-S. Lee, M. Meyyappan, Synthesis and characterization of carbon nanowalls on different substrates by radio frequency plasma enhanced chemical

vapor deposition, Carbon 72 (2014) 372-380. https://doi.org/10.1016/j.carbon.2014.02.025.

[36] J. Zhang, J. Xiao, X. Meng, C. Monroe, Y. Huang, J. Zuo, Quantitative Analysis of Graphene Folded Edges Using Electron Diffraction, Microscopy and Microanalysis 16(S2) (2010) 1482-1483. https://doi.org/10.1017/s1431927610056412.

[37] P. Delhaes, Chemical vapor deposition and infiltration processes of carbon materials, Carbon 40 (2014) 641-657. https://doi.org/10.1016/S0008-6223(01)00195-6.

[38] J. Hu, J. Zhang, G. Luo, Y. Sun, Q. Shen, L. Zhang, Effectively enhanced strength by interfacial reactions in in-situ carbon reinforced Al matrix composites, Vacuum 188 (2021) 110148. https://doi.org/10.1016/j.vacuum.2021.110148.

[39] Z. Huang, J. Li, J. Yao, H. Zhou, Y. Huang, L. Wang, F. Zheng, Characterization of CNT–pyrolytic C-layer-coated Al foil: interfacial structures, reactions, and performances, Applied Physics A 123(11) (2017) 687. https://doi.org/10.1007/s00339-017-1312-8.

[40] L.X. Zhang, Z. Sun, J.L. Qi, J.M. Shi, T.D. Hao, J.C. Feng, Understanding the growth mechanism of vertically aligned graphene and control of its wettability, Carbon 103 (2016) 339-345. https://doi.org/10.1016/j.carbon.2016.03.029.

[41] Z. Huang, J. Li, J. Yao, H. Zhou, Y. Huang, L. Wang, Structures and interfaces of CNT: pyrolytic C coated Al foil and its performance as current collector of electrochemical double layer capacitor, Journal of Materials Science: Materials in Electronics 28(20) (2017) 15095-15105. https://doi.org/10.1007/s10854-017-7385-5.

Declaration of interests

☒The authors declare that they have no known competing financial interests or personal relationships that could have appeared to influence the work reported in this paper.

☐The authors declare the following financial interests/personal relationships which may be considered as potential competing interests: